Metabolomics (2014) 10:663–676
DOI 10.1007/s11306-013-0594-x

ORIGINAL ARTICLE

MS-based metabolite profiling reveals time-dependent skin biomarkers in UVB-irradiated mice

Hye Min Park · Jung-Hoon Shin · Jeong Kee Kim · Sang Jun Lee · Geum-Sook Hwang · Kwang-Hyeon Liu · Choong Hwan Lee

Received: 19 August 2013 / Accepted: 15 October 2013 / Published online: 26 October 2013

Abstract We observed clinical and histological changes, including increased transepidermal water loss, epidermal thickness, and inflammatory cells, and changes in collagen fibers in the skin of mice chronically exposed to ultraviolet (UV) B radiation for 12 weeks. By using ultra-performance liquid chromatography-quadrupole time-of-flight (TOF) mass spectrometry (MS), gas chromatography (TOF–MS), and NanoMate tandem-MS-based metabolite profiling, we identified amino acids, organic compounds, fatty acids, lipids, nucleosides, carbohydrates, lysophosphatidylcholines, lysophosphatidylethanolamines, urocanic acids, and ceramides (CERs) as candidate biomarkers of the histological changes in mouse skin following UVB irradiation for 6 and 12 weeks. *cis*-Urocanic acid and cholesterol showed the most dramatic increase and decrease at 6 and 12 weeks, respectively. In addition, the changes in skin primary metabolites and lysophospholipids induced by UVB exposure were generally greater at 12 weeks than at 6 weeks. The results from primary metabolite, lysophospholipid, and CER profiles suggest that prolonged chronic exposure to UVB light has a great effect on skin by altering numerous metabolites. A comprehensive MS-based metabolomic approach for determining regulatory metabolites in UV-induced skin will lead to a better understanding of the relationship between skin and UV.

Keywords Cholesterol · Mass spectrometry · Metabolite profiling · Skin · *cis*-Urocanic acid · UVB

Electronic supplementary material The online version of this article (doi:10.1007/s11306-013-0594-x) contains supplementary material, which is available to authorized users.

H. M. Park · C. H. Lee (✉)
Department of Bioscience and Biotechnology, Kon-Kuk University, 120 Neungdong-ro, Gwangjin-gu, Seoul 143-701, Republic of Korea
e-mail: chlee123@konkuk.ac.kr

J.-H. Shin · K.-H. Liu
College of Pharmacy and Research Institute of Pharmaceutical Sciences, Kyungpook National University, 80 Daehak-ro, Buk-gu, Daegu 702-701, Republic of Korea

J. K. Kim · S. J. Lee
Food Research Institute, AmorePacific R&D Center, 1920 Yonggu-daero, Giheung-gu, Yongin, Gyeonggi-do 446-729, Republic of Korea

G.-S. Hwang
Integrated Metabolomics Research Group of Seoul Center, Korea Basic Science Institute, Seoul 136-701, Republic of Korea

1 Introduction

Chronic exposure of the skin to ultraviolet (UV) radiation, including UVA and UVB, induces clinical and histological damage that results in skin destruction and repair proceeding simultaneously (Berneburg et al. 2000; Legat and Wolf 2006). In the hairless mouse, a relevant model for the systematic study of photoaging (Kligman 1989), UVB radiation damages connective tissue more efficiently than any other longer wavelength radiation (Chaqour et al. 1997). Most previous studies on photodamaged skin focused on morphological and histological changes, such as wrinkles and connective-tissue alterations, using biochemical and molecular biological techniques. However, with technical advances in analytic instruments and highly efficient mass spectroscopy, metabolomics has been used more frequently in recent studies to discover new metabolic biomarkers for the diagnosis of diseases (Boros et al. 2003; Hu et al. 2009). Few recent researches have investigated the metabolic changes induced by ionizing radiation

in cell lines and rat plasma (Varghese et al. 2010; Liu et al. 2013). Furthermore, metabolomics was recently reported as a novel approach for detecting volatile metabolites in the skin and melanoma after UV exposure, a known risk factor for melanoma (Abaffy et al. 2010; Narayanan et al. 2010). Despite many physiological evidence-based molecular mechanism studies of the relationship between the skin and UV radiation, metabolite profiling of skin after UV radiation has not yet been performed.

Identifying skin metabolites that change according to UV exposure is necessary to understand the effect of UV irradiation on the skin in detail. Because there are limitations to analyzing all metabolites using a single instrument, a combination of high-throughput techniques, such as nuclear magnetic resonance spectroscopy and mass spectrometry (MS), is required to identify a wide range of metabolites. The improved sensitivity and resolution of MS permits greater coverage of the metabolome, resulting in the increased use of MS-based metabolomic techniques. The two predominant MS-based analytical methods are liquid chromatography and gas chromatography coupled with MS (i.e., LC–MS and GC–MS, respectively) (Dehaven et al. 2010). GC–MS is an effective combination for the analysis of less polar compounds, such as essential oils, free fatty acids, steroids, diglycerides, mono-, di-, and trisaccharides, and sugar alcohols. Because LC separates metabolites that are not volatile and are not derivatized, LC–MS can analyze a much wider range of chemical species than GC–MS (Halket et al. 2005). With the combination of LC–MS and GC–MS, multivariate analysis tools must be used to visualize the metabolites among the experimental groups and to analyze the statistical significance of the data, because large volumes of highly variable data are typically collected from an MS measurement (Kim et al. 2012; Lee et al. 2012).

In this study, metabolites in mouse skin, including lysophospholipids, primary metabolites, and ceramides (CERs), after UVB irradiation for 6 and 12 weeks were profiled using ultra-performance liquid chromatography (UPLC)-quadrupole time-of-flight (Q-TOF)-MS, GC–TOF–MS, and chip-based nanoelectrospray tandem-MS analyses with multivariate statistical analysis, respectively. Metabolites that discriminated non-irradiated skin from UV-irradiated skin, depending on UVB exposure time, were tentatively identified.

2 Materials and methods

2.1 Reagents

Methanol, water, and acetonitrile were purchased from Fisher Scientific (Pittsburgh, PA, USA). Ammonium acetate, formic acid, dichloromethane, methoxyamine hydrochloride, and *N*-methyl-*N*-(trimethylsilyl)trifluoroacetamide (MSTFA) were obtained from Sigma Chemical Co. (St. Louis, MO, USA). Synthetic CERs were purchased from Avanti Polar Lipids (Alabaster, AL, USA) or Matreya (Pleasant Gap, PA, USA). All chemicals and solvents were of analytical grade.

2.2 Animals

A relevant model for the systematic study of photoaging, the hairless mouse develops a typical reaction to chronic UV radiation, characterized by elastic fiber hyperplasia and followed by elastosis and ultrastructural degradation (Kligman 1989). Six-week-old female albino hairless mice (Skh:hr-1) were obtained from Charles River Laboratories (Wilmington, MA, USA). The animals were acclimatized for 1 week in an animal facility prior to the experiments and housed under controlled conditions of temperature (23 ± 2 °C), relative humidity (55 ± 10 %), and light (12-h light/dark cycle). The animals had free access to a laboratory diet (Purina, St. Louis, MO, USA) and ion sterilized tap water. The experiment was performed in accordance with the guidelines of The AmorePacific Institutional Animal Care and Use Committee and the OECD "Guide for the Care and Use of Laboratory Animals."

2.3 Experimental design

The hairless mice were weight-matched and divided into two groups, with 20 mice in each group: normal control (NC) group and UVB-irradiated control (UC) group. We used ten fluorescent lamps (TL 20 W/12RS, peak emission 320 nm, wavelength 275–390 nm; Philips, Amsterdam, Netherlands), and the UVB emission was monitored with a UV radiometer (VLX-3W; Vilber Lourmat, Marne-la-Vallée, France). The mice in the UC group were exposed to UVB radiation three times a week. One minimal erythema dose (MED; 55 mJ/cm^2) was administered during the first week; this was then increased by one MED per week until 4 weeks, after which the mice were exposed to four MED for the duration of the experiment. The irradiation intensity was measured at the bottom of the cage, and the animals were able to move around freely in the cage during the period of exposure in a steel irradiation chamber (Son et al. 2007). After exposure to UVB radiation during weeks 6 and 12, ten mice in each group were sacrificed by cervical dislocation, and skin samples were collected.

2.4 Clinical and histological assessment

The transepidermal water loss (TEWL) was determined using a VapoMeter (Delfin Technologies Ltd., Kuopio,

Finland) in 50 ± 5 % relative humidity and at 23.5 ± 0.5 °C, and the values were presented as g/m^2 h. The viable folding thickness was measured using a micrometer (Absolute, Mitutoyo, Japan) using the back skin of the hairless mice. For histology, dorsal skin tissues were fixed in 10 % neutral phosphate-buffered formalin, processed in a routine manner, embedded in paraffin, sectioned at 3-μm thickness, and stained with hematoxylin and eosin (H&E). Sections sequentially cut from collected samples were used for Masson's trichrome staining to evaluate collagen in the dermis. All stained sections were examined under a light microscope (BX41; Olympus, Tokyo, Japan), and photomicrographs were taken with a DP72 digital camera (Olympus, Tokyo, Japan).

2.5 Sample preparation

Skin specimens (area: 2 × 3 cm) from the central dorsum of mice were chopped finely before solvent extraction. Methanol (600 μL) was added to the skin tissues, which were then homogenized (30-s frequency) three times for 5 min at room temperature using a mixer mill MM400 (Retsch®, Haan, Germany). The suspension was centrifuged at 4 °C and 12,000 rpm for 10 min, and the resulting supernatant (aqueous extract) was evaporated with a speed-vacuum machine. Dried samples were resuspended with methanol for UPLC-Q-TOF–MS analysis. For GC–TOF–MS analysis, the skin extracts were oximated with 50 μL of methoxyamine hydrochloride (20 mg/mL) in pyridine at 30 °C for 90 min, silylated with 50 μL of MSTFA, and then incubated at 37 °C for 30 min. All samples were prepared at the same concentration to normalize for different amounts of tissue. The final concentrations of the analyzed samples were 2.5 and 10 mg/mL, respectively.

To determine the change in CERs in UVB-irradiated skin, the remaining pellets were extracted twice with 600 μL of a solvent mixture (dichloromethane:methanol, 2:1). The supernatants (organic extracts) were collected and evaporated. Dried samples were reconstituted with dichloromethane and diluted with a methanol and chloroform solvent mixture (9:1, v/v) containing 7.5 mM ammonium acetate to obtain a final concentration of 0.1 mg/mL. An in-house quality control sample was prepared by pooling and mixing the same concentration of each sample.

2.6 GC–TOF–MS analysis and data processing

To study the changes in primary metabolites such as amino acids, fatty acids, and saccharides induced by exposure of skin to UVB radiation, GC–TOF–MS analysis was performed on an Agilent 7890 GC system (Agilent, Atlanta, GA) coupled with a Pegasus® HT TOF–MS (Leco Corp., St. Joseph, MI, USA) using an Agilent 7693 autosampler (Agilent, Atlanta, GA). The system was equipped with an Rtx-5MS column (29.8 m × 0.25 mm i.d., particle size of 0.25 μm; Restek Corp., Bellefonte, PA, USA). The front inlet and transfer line temperatures were set at 250 and 240 °C, respectively. The helium gas flow rate through the column was 1.5 mL/min, and ions were generated by a 70 eV electron impact (EI). The ion source temperature was set at 230 °C, and the mass range was 50–800 *m/z*. The column temperature was maintained isothermally at 75 °C for 2 min, increased to 300 °C at a rate of 15 °C/min, and then maintained at 300 °C for 3 min. One microliter of reactant was injected into the GC–TOF–MS with a split ratio of 10:1. For quantitative analysis of major skin biomarker candidates, including *trans*- and *cis*-urocanic acid (UCA) and cholesterol, skin samples were analyzed using GC–TOF–MS under the same conditions.

The data processing for GC–TOF–MS was performed using ChromaTOF™ software (Leco Corp., St. Joseph, MI, USA), and raw data files were converted to the network common data form (netCDF, *.cdf). After conversion, the MS data were processed using the MetAlign software package (http://www.metalign.nl) to obtain a data matrix containing retention times, accurate masses, and normalized peak intensities. The resulting data were exported to Microsoft Excel (Microsoft, Redmond, WA, USA). Between the NC and UC groups, 9,170 and 12,248 variables were detected according to UVB exposure time at 6 and 12 weeks, respectively, and were used for multivariate analysis.

2.7 UPLC-Q-TOF–MS analysis and data processing

To study the changes in phospholipids in the skin induced by UVB exposure, UPLC-Q-TOF–MS was performed on a Waters Q-TOF Premier (Micromass MS Technologies, Manchester, UK) with a Waters Acquity UPLC System (Waters Corp., Milford, MA, USA) equipped with a Waters Acquity HPLC BEH C_{18} column (100 × 2.1 mm i.d., particle size of 1.7 μm). The samples were separated using a linear gradient consisting of water (A) and acetonitrile (B) with 0.1 % v/v formic acid under the following conditions: 5 % B for 1 min; gradually increased to 55 % B over 4 min; increased to 100 % B for 8 min; maintained at 100 % B for 1 min; and then decreased to 5 % B over 1 min. The injection volume of sample was 5 μL, and the flow rate was maintained at 0.3 mL/min. The TOF–MS data was collected in the range of 100–1,000 *m/z* with a scan time of 0.2 s and an interscan time of 0.02 s in negative ion mode. The capillary and cone voltages were set at 3.0 kV and 40 V, respectively. The desolvation gas flow was set to 600 L/h at a temperature of 200 °C, and the cone gas flow was set to 50 L/h. The ion source temperature was 200 °C.

UPLC-Q-TOF–MS data processing was performed with MassLynx software, and raw data files were converted into netCDF (*.cdf) format with Waters DataBridge version 2.1 software. After conversion, the MS data were processed under the same data processing method as GC–TOF–MS. According to UVB exposure time, 472 and 457 variables were detected between the NC and UC groups at 6 and 12 weeks, respectively, and were used for multivariate analysis.

2.8 Ceramide analysis and data processing

To study changes in CERs in skin induced by UVB exposure, we performed target CER profiling using an LTQ XL mass spectrometer (Thermo Fisher Scientific, West Palm Beach, FL, USA) equipped with a TriVersa NanoMate robotic nanoflow ion source (Advion Biosciences, Ithaca, NY, USA) and nanoelectrospray chips with spraying nozzles 5.5 μm in diameter. The ion source was controlled by Chipsoft 8.3.1 software (Advion Biosciences). The ionization voltage was −1.45 kV in negative mode; backpressure was set at 0.4 psi. The temperature of the ion transfer capillary was 200 °C; the tube voltage was −100 V. Under these settings, 10 μL of the analyte could be electrosprayed for more than 50 min.

For the analysis, 10 μL of sample was loaded onto a 96-well plate (Eppendorf, Hamburg, Germany) of the TriVersa NanoMate ion source, which was then sealed with aluminum foil. Each sample was analyzed for 2 min. The data collection method performed a full scan (scan range: *m/z* 400–1,000) and a data dependent MS/MS scan of the most abundant ions. Standard spectra were scanned in low-resolution mode with 30 eV CID voltage to obtain specific MS/MS fragmentations. All spectra were recorded with Thermo Xcalibur software (version 2.1; Thermo Fisher Scientific, West Palm Beach, FL, USA).

MS data obtained from the ion trap mass spectrometer were aligned using the MATLAB software (version 8.0; MathWorks, Natick, MA, USA) directly from raw files to obtain a data matrix containing 601 variables with *m/z* values and peak intensities for multivariate analysis. Additionally, skin CERs were tentatively identified based on their specific MS/MS fragmentation pattern, and only identified CERs were used for multivariate analysis.

2.9 Multivariate statistical analysis

Multivariate statistical analysis was performed using principal component analysis, partial least squares discriminant analysis (PLS-DA) (Fig. S1 and Table S1), and orthogonal partial least square (OPLS)-DA from SIMCA-P + software (version 12.0; Umetrics, Umea, Sweden). The potential variables were selected based on variable importance in the projection (VIP) and *p* values using SIMCA-P + software and Statistica 7 (StatSoft Inc., Tulsa, OK, USA). After the multivariate statistical analysis, the corresponding peaks of the selected variables were confirmed in the original chromatogram and were positively/tentatively identified using commercial standard compounds in comparison with the mass spectra and retention time or on the basis of the Human Metabolome Database (HMDB; http://www.hmdb.com), Lipid Maps Databases (http://www.lipidmaps.org), National Institute of Standards and Technology (NIST) mass spectral database (FairCom, Gaithersburg, MD, USA), and references.

3 Results

3.1 Clinical observations and histopathology

There were significant differences in TEWL and viable folding thickness between NC and UC groups at week 12 of UVB irradiation (Fig. 1a, b). TEWL in the UC group was elevated by 96.8 % compared to that in the NC group ($p = 0.000$). The viable folding thickness was also increased in the UC group by 23.4 % ($p = 0.000$). In the UC group, there were also definite differences in skin histology. Degenerated epidermis with multi-focally erosive or ulcerated lesions was covered with thick serocellular crusts and accompanied by hypertrophy of keratinocytes. Moderate numbers of inflammatory cells, predominantly neutrophils and some lymphocytes, infiltrated the multi-focally exposed superficial dermis, which was expanded with edema and hemorrhage. The dermis was diffused throughout with increased numbers of inflammatory cells around the blood vessels (Fig. 1c, d, arrow). Finally, compared to normal blue collagen bundles, the collagen fiber bundles in the UC group were distorted, shorter, and thinner with turbid discoloration (Fig. 1e, f, star).

3.2 Significantly altered primary metabolites according to UVB irradiation status identified by GC–TOF–MS analysis

Primary skin metabolite profiles in response to UVB irradiation were analyzed by the OPLS-DA model to identify discriminable variables between the two experimental groups. The OPLS-DA score plots of the NC and UC groups were clearly divided according to UVB irradiation (Fig. 2a, c) based on the model with R^2X_{cum} and R^2Y_{cum} values and with Q^2_{cum} (Table S1). S-plots were generated to visualize the variables, selected by the VIP value (>0.7) and *p* value (<0.05), that significantly contributed to the discrimination between the experimental groups (Fig. 2b, d). The variables identified are summarized in Table 1. Amino acids, organic compounds, fatty acids, lipids,

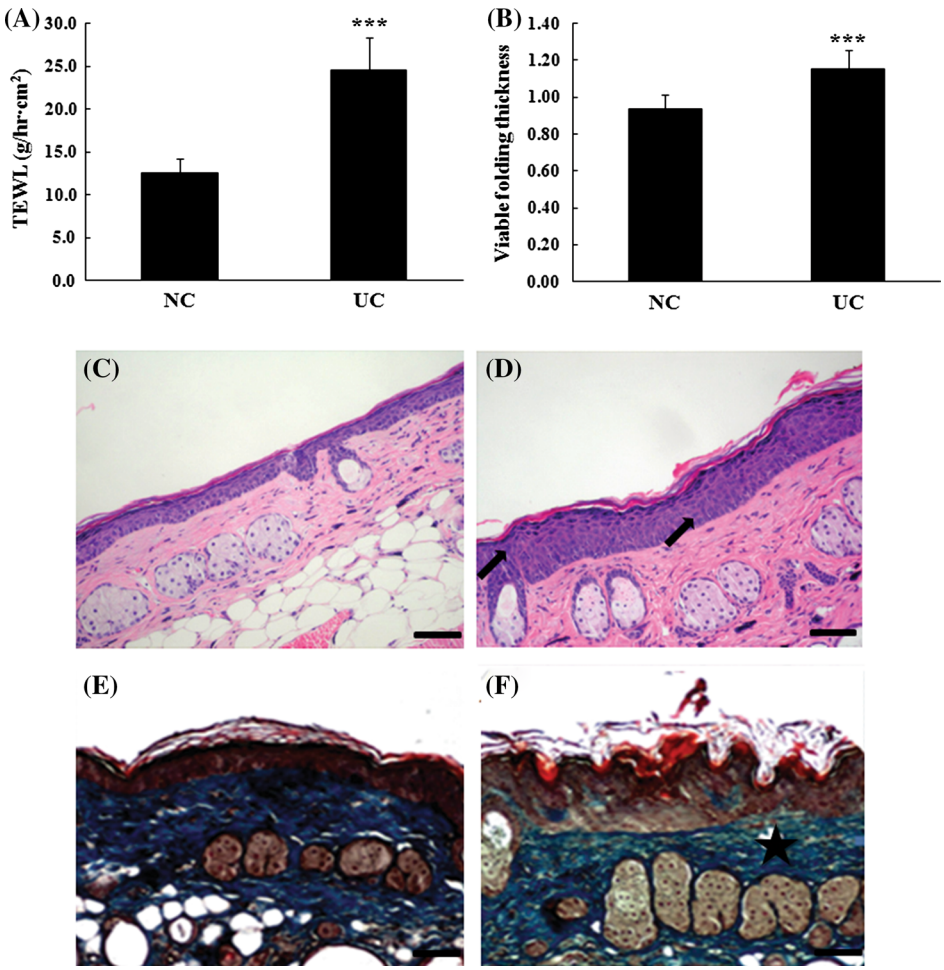

Fig. 1 TEWL (**a**), epidermal thickness (**b**), histological appearance (**c**, **d**), and Masson's trichrome staining (**e**, **f**) of hairless mouse skin from the NC (**c**, **e**) and UC (**d**, **f**) groups after UVB irradiation for 12 weeks. *Asterisks* indicate statistically significant differences from the UC group (***$p < 0.001$). *Bar* 30 μm (**c**, **d**), 24 μm (**e**, **f**)

nucleosides, carbohydrates, and *cis*- and *trans*-UCA were identified as discriminators that characterized the differences between the groups. After UVB exposure for 6 weeks, *cis*-UCA showed the most dramatic increase. The levels of amino acids and nucleosides, including uridine and cytidine, were increased, whereas the level of *trans*-UCA was decreased, by exposure to UVB radiation for 6 and 12 weeks. Citric acid and histamine increased after exposure to UVB radiation for 6 weeks, but these metabolites decreased in the dorsal skin of UVB-irradiated mice after 12 weeks. After long-term exposure to UVB for 12 weeks, carbohydrates and fatty acids, as well as hypoxanthine and inosine, molecules related to purine metabolism, declined in UVB-irradiated mice. The levels of cholesterol and lathosterol were reduced 0.26- and 0.35-fold, respectively, by exposure to UVB radiation for 12 weeks. *cis*-UCA and cholesterol showed the most dramatic changes at 6 and 12 weeks, respectively; the changes are quantified in Table S2. These results indicate that chronic exposure to UVB for 12 weeks had a greater impact on a larger number of primary metabolites than exposure to UVB for 6 weeks.

3.3 Significantly altered lysophospholipids according to UVB irradiation status identified by UPLC-Q-TOF–MS analysis

OPLS-DA was successfully applied to the lysophospholipid profiles of the dorsal skin of mice in response to UVB light obtained by UPLC-Q-TOF–MS analysis. The score plots of OPLS-DA showed a clear differentiation between the NC and UC groups depending on the period of exposure to UVB rays (Fig. 2e, g) based on the model with R^2X_{cum} and R^2Y_{cum} values and with Q^2_{cum} (Table S1). The S-plots were generated from these OPLS-DA models to screen the metabolites responsible for the separation between groups (Fig. 2f, h). Assignment of metabolites contributing to the observed variance was performed by elemental composition analysis software with calculated mass, mass tolerance (mDa and ppm), double bond equivalent (DBE), and iFit algorithm implemented in the MassLynx and by HMDB. Four (6 weeks) and eight (12 weeks) metabolites were tentatively identified as potential biomarkers for the diagnosis of damaged skin following UVB exposure. Lysophosphatidylcholines

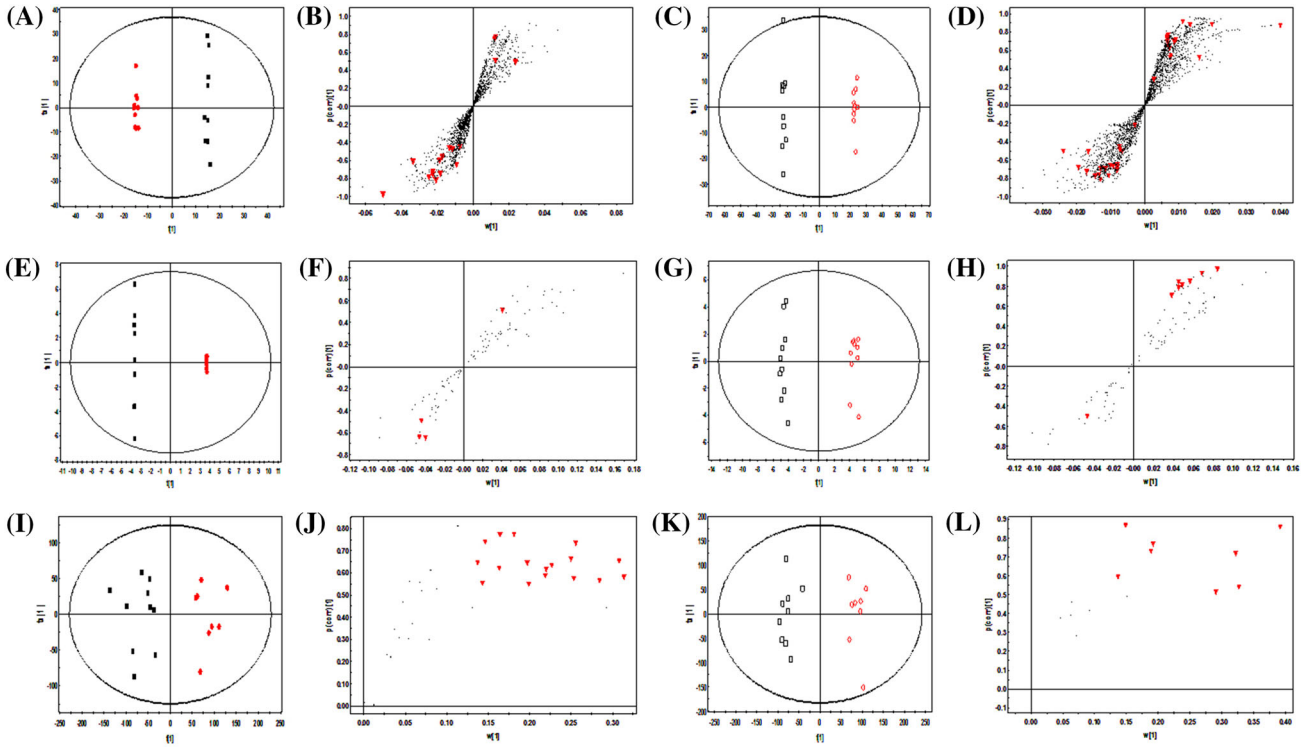

Fig. 2 OPLS-DA score plots from the GC–TOF–MS (**a**–**d**), UPLC-Q-TOF–MS (**e**–**h**), and NanoMate LTQ-MS (**i**–**l**) data sets with corresponding S-plots for the aqueous extracts of mouse skin after exposure to UVB radiation. (**a**, **e**, **i**) OPLS-DA score plots from the NC and UC groups after 6 weeks; (**c**, **g**, **k**) OPLS-DA score plots from the NC and UC groups after 12 weeks; (**b**, **f**, **j**) potential biomarkers in the S-plot between the NC and UC groups after 6 weeks; (**d**, **h**, **l**) potential biomarkers in the S-plot between the NC and UC groups after 12 weeks. *Filled square* 6 weeks, NC; *filled circle* 6 weeks, UC; *open square* 12 weeks, NC; *open circle* 12 weeks, UC. The selected variables (*filled down pointing triangle*, VIP > 0.7 and $p < 0.05$) are highlighted in the S-plots

(lysoPCs) exist in two forms (*sn*-1 and *sn*-2) that differ in the position of the fatty acyl group, and the two lysoPC forms were found in our skin samples. In UVB-irradiated skin after 6 weeks, lysoPC 22:6 and the two forms of lysoPC 18:0 were lower than in normal skin, whereas lysophosphatidylethanolamine (lysoPE) 18:2 higher. After 12 weeks, UVB-induced skins had significantly increased levels of eight metabolites, but not lysoPC 18:0 (Table 2). We observed that the changes in skin metabolites induced by UVB exposure were generally higher at 12 weeks than at 6 weeks. The results from primary metabolite and lysophospholipid profiles suggest that prolonged chronic exposure to UVB light has a great influence on skin by altering its metabolites, both negatively and positively.

3.4 Significantly altered skin CERs according to UVB irradiation status identified by NanoMate-LTQ analysis

The targeted MS/MS analysis obtained by NanoMate-LTQ provided information on the specific fragment ions of the acyl and sphingoid units, which are informative for the structural identification of CERs. Using synthetic CER standards [NS (*m/z* 550), NdS (*m/z* 650), AS (*m/z* 608), AdS (*m/z* 582), and NP (*m/z* 554)] as an example, the identification procedure is illustrated step-by-step in the Supplementary Material (Fig. S2). By using this approach, 36 CERs—including members of all six classes NS, NdS, NP, NH, AS, and AdS—were identified, as presented in Table S3.

The 36 CERs identified from the MS/MS data of skin organic extracts were applied to OPLS-DA score plots (Fig. 2i, k). Each group was clearly discriminated based on the model with R^2X_{cum} and R^2Y_{cum} values and with Q^2_{cum} (Table S1). To determine which CERs contributed to the discrimination between non-irradiated and UVB-irradiated skin, S-plots were generated using Pareto scaling (Fig. 2j, l). After 6 and 12 weeks, the selected skin CERs showed significant alterations, increasing between 1.33- and 2.46-fold (Table 3). In contrast to the changes observed in primary and secondary metabolites, the number of CERs significantly altered by UVB exposure was higher at 6 weeks than at 12 weeks.

Table 1 Primary metabolites significantly altered between NC and UC groups after exposure to UVB radiation for 6 and 12 weeks, as identified by GC–TOF–MS analysis

t_R (min)	Identified ion (*m/z*)	Metabolites	Derivatized	Fold change[a]	VIP	*p* value	ID
6 weeks							
Amino acids							
9.89	227	L-Glutamine	TMS (X 2)	0.76	1.20	0.024	STD/MS[b]
11.20	156	L-Glutamine	TMS (X 3)	3.22	3.22	0.004	STD/MS
11.53	142	DL-Ornithine	TMS (X 4)	1.95	2.15	<0.001	STD/MS
12.23	156	L-Lysine	TMS (X 4)	1.17	0.71	0.043	STD/MS
12.26	254	L-Histidine	TMS (X 3)	1.75	1.99	<0.001	STD/MS
12.36	218	L-Tyrosine	TMS (X 3)	1.20	0.90	0.002	STD/MS
14.15	202	L-Tryptophan	TMS (X 3)	1.60	1.76	<0.001	STD/MS
Organic compounds							
10.48	326	Taurine	TMS (X 3)	0.60	2.26	0.026	STD/MS
11.56	273	Citric acid	TMS (X 4)	1.60	1.62	0.008	STD/MS
11.92	174	Histamine	TMS (X 3)	1.78	1.80	0.005	STD/MS
Fatty acids							
13.54	117	Heptadecanoic acid	TMS (X 1)	1.32	1.13	0.030	STD/MS
16.22	117	Docosanoic acid	TMS (X 1)	1.42	1.28	0.038	STD/MS
Nucleobase							
15.41	224	Uridine	TMS (X 4)	2.14	2.36	<0.001	STD/MS
16.67	223	Cytidine	TMS (X 4)	2.18	2.16	<0.001	STD/MS
Carbohydrates							
13.42	217	*myo*-Inositol	TMS (X 6)	0.84	1.14	<0.001	STD/MS
Others							
11.19	267	*cis*-Urocanic acid	TMS (X 3)	–	4.82	<0.001	STD/MS
12.74	267	*trans*-Urocanic acid	TMS (X 3)	0.84	1.19	<0.001	STD/MS
12 weeks							
Amino acids							
6.47	144	L-Valine	TMS (X 2)	1.20	0.72	<0.001	STD/MS
9.89	227	L-Glutamine	TMS (X 2)	1.61	1.48	<0.001	STD/MS
10.05	246	Glutamic acid	TMS (X 3)	1.15	0.76	<0.001	STD/MS
10.14	218	Phenylalanine	TMS (X 2)	1.13	0.73	0.001	STD/MS
10.46	116	L-Asparagine	TMS (X 3)	1.19	0.80	0.003	STD/MS
10.70	84	L-Lysine	TMS (X 3)	1.65	1.78	0.021	STD/MS
11.53	142	DL-Ornithine	TMS (X 4)	1.32	0.84	0.023	STD/MS
12.23	156	L-Lysine	TMS (X 4)	1.12	0.73	<0.001	STD/MS
12.26	254	L-Histidine	TMS (X 3)	1.33	0.99	0.001	STD/MS
Organic compounds							
6.13	261	Urea	TMS (X 3)	0.34	1.84	0.022	STD/MS
7.69	245	Fumaric acid	TMS (X 2)	1.31	1.24	<0.001	STD/MS
9.93	188	Hypotaurine	TMS (X 3)	1.23	0.94	0.001	STD/MS
11.56	273	Citric acid	TMS (X 4)	0.51	1.62	<0.001	STD/MS
11.92	174	Histamine	TMS (X 3)	0.77	0.90	0.001	STD/MS
Fatty acids and lipids							
12.94	75	Palmitic acid	TMS (X 1)	0.75	0.75	0.019	STD/MS
14.12	341	Stearic acid	TMS (X 1)	0.64	1.18	<0.001	STD/MS
14.88	75	Arachidonic acid	TMS (X 1)	0.84	2.65	0.022	STD/MS
15.10	338	*cis*-Oleamide	TMS (X 1)	0.69	1.13	0.001	STD/MS
15.89	117	Docosahexaenoic acid	TMS (X 1)	0.56	1.44	<0.001	STD/MS

Table 1 continued

t_R (min)	Identified ion (*m/z*)	Metabolites	Derivatized	Fold change[a]	VIP	*p* value	ID
16.01	371	Monopalmitin	TMS (X 2)	0.71	1.03	0.001	STD/MS
16.22	117	Docosanoic acid	TMS (X 1)	0.54	1.45	0.001	STD/MS
16.84	129	Monoolein	TMS (X 2)	0.63	0.82	0.043	STD/MS
19.35	129	Cholesterol	TMS (X 1)	0.26	4.42	<0.001	STD/MS
19.82	255	Lathosterol	TMS (X 1)	0.35	1.90	<0.001	STD/MS
Nucleobase							
11.46	265	Hypoxanthine	TMS (X 2)	0.54	1.49	<0.001	STD/MS
15.41	224	Uridine	TMS (X 4)	1.25	0.85	0.012	STD/MS
16.06	217	Inosine	TMS (X 4)	0.50	1.62	<0.001	STD/MS
16.67	223	Cytidine	TMS (X 4)	3.11	2.18	<0.001	STD/MS
Carbohydrates							
12.18	205	Glucose	TMS (X 5)	0.61	1.27	0.001	STD/MS
13.42	217	*myo*-Inositol	TMS (X 6)	0.77	0.91	<0.001	STD/MS
17.02	204	Maltose	TMS (X 8)	0.26	2.17	0.001	STD/MS
Others							
12.74	267	*trans*-Urocanic acid	TMS (X 3)	0.77	0.90	0.001	STD/MS

Variables were selected by VIP value (>0.7) and *p* value (<0.05) from OPLS-DA models

t_R retention time, *VIP* variable important in the projection, *ID* identification

[a] Fold change was calculated by dividing the mean of the peak area of the identified ion MS fragment (*m/z*) of each metabolite from the UVB-irradiated group by that of the normal group

[b] Metabolites were identified using commercial standard compounds (STD) in comparison with the mass spectra (MS) and retention time

4 Discussion

In this study, when mice were chronically irradiated with UVB rays for 12 weeks, TEWL, viable epidermal thickness, and the number of inflammatory cells increased in UVB-exposed skin (Fig. 1). Photodamaged skin frequently displays variable epidermal thickness, dermal elastosis, decreased/fragmented collagen, increased matrix-degrading metalloproteinases, inflammatory infiltrates, and vessel ectasia. Moloney et al. (1992) demonstrated that when Skh-1 hairless mice were irradiated with suberythemal doses of UVB three times a week, visible wrinkling and increased epidermal thickness were present after 6–7 weeks of irradiation, and dermal thickening was evident after 10 weeks of irradiation. Additionally, using GC–TOF–MS, UPLC-Q-TOF–MS, and NanoMate-LTQ analysis, we found that many different kinds of skin metabolites, including amino acids, organic compounds, fatty acids, sterols, nucleosides, carbohydrates, lysoPCs, lysoPEs, UCA, and CERs, were altered in mouse skin in a manner dependent on the UVB exposure period. The changes in skin primary metabolites and lysophospholipids by UVB exposure were generally greater at 12 weeks than at 6 weeks (Fig. S3).

Free amino acids are a major portion of the natural moisturizing factors present in the stratum corneum (SC), the outermost layer of the epidermis in skin. Arg, Gln, Gly, Pro, Orn, and Lys stimulate collagen synthesis and wound collagen accumulation (Bellon et al. 1995; Shi et al. 2002; Dioguardi 2008). Svobodova et al. (2006) demonstrated that Trp, Tyr, Phe, His, and Cys are UV-absorbing cellular chromophores that produce superoxide anions by photo-oxidation. In our data, chronic UVB irradiation for 6 and 12 weeks tended to increase the levels of most amino acids, suggesting that altered levels of the free amino acids influenced epidermal thickness, water binding capacity, and reactive oxygen species (ROS) production.

Together with amino acids, UCA and histamine, molecules associated with histidine metabolism, were detected in mouse dorsal skin exposed to UVB radiation. UCA is a metabolic product of filaggrin, a histidine-rich protein. UCA is present in the *trans*-form in the epidermis. Following absorption of UV radiation, UCA photoisomerizes from the naturally occurring *trans*-isomer to the *cis*-isomer. *cis*-UCA serves as an important mediator of UV-induced immunosuppression, affecting immune cell proliferation and the generation of extracellular superoxide and cytokines (Norval et al. 1989; Lappin et al. 1995; Gibbs et al. 2008). Because exposure to UVB light for 6 weeks induced photoisomerization of *trans*-UCA, the amount of *cis*-UCA was significantly higher in UVB-exposed skin than in

Table 2 Lysophospholipids significantly altered between NC and UC groups after exposure to UVB radiation for 6 and 12 weeks, as identified by UPLC-Q-TOF–MS analysis

t_R (min)	Tentative metabolites[a]	Measured MS (*m/z*)	HMDB formula	error (mDa)	Adduct	Fold change[b]	VIP	*p* value
6 weeks								
7.90	LysoPC 22:6	612.3297	$C_{30}H_{50}NO_7P$	−0.4	M+FA−H [1−]	0.80	1.02	0.002
7.94	LysoPE 18:2	476.2772	$C_{23}H_{44}NO_7P$	−0.5	M−H [1−]	1.23	0.89	0.023
10.02	LysoPC 18:0*	568.3617	$C_{26}H_{54}NO_7P$	0.3	M+FA−H [1−]	0.80	0.97	0.027
10.37	LysoPC 18:0*	568.3605	$C_{26}H_{54}NO_7P$	−0.9	M+FA−H [1−]	0.86	0.87	0.002
12 weeks								
7.54	LysoPC 16:1	538.3148	$C_{24}H_{48}NO_7P$	0.3	M+FA−H [1−]	1.30	0.96	<0.001
7.74	LysoPC 18:2*	564.3283	$C_{26}H_{50}NO_7P$	−1.8	M+FA−H [1−]	1.49	1.21	<0.001
7.94	LysoPE 18:2	476.2756	$C_{23}H_{44}NO_7P$	−2.1	M−H [1−]	2.10	1.79	<0.001
8.00	LysoPC 18:2*	564.3302	$C_{26}H_{50}NO_7P$	0.1	M+FA−H [1−]	1.67	1.46	<0.001
8.95	LysoPE 18:1	478.2939	$C_{23}H_{46}NO_7P$	0.5	M−H [1−]	1.29	0.96	<0.001
9.00	LysoPC 18:1	566.3458	$C_{26}H_{52}NO_7P$	1.4	M+FA−H [1−]	1.34	1.04	<0.001
9.48	LysoPE 20:0	554.3455	$C_{25}H_{52}NO_7P$	−0.3	M+FA−H [1−]	1.24	0.81	0.001
10.02	LysoPC 18:0	568.3622	$C_{26}H_{54}NO_7P$	0.8	M+FA−H [1−]	0.71	1.00	0.017

Variables were selected by VIP value (>0.7) and *p* value (<0.05) from OPLS-DA models.

HMDB The Human Metabolome Data Base (http://www.hmdb.ca/), *FA* formic acid, *LysoPC* lysophosphatidylcholine, *LysoPE* lysophosphatidylethanolamine, t_R retention time, *VIP* variable important in the projection

Asterisk means the two forms of lysoPC, with the fatty acyl groups at positions 1 (*sn*-1) or 2 (*sn*-2) on the glycerol backbone

[a] Assignment of metabolites contributing to the observed variance was performed by elemental composition analysis software with calculated mass, mass tolerance (mDa and ppm), DBE, and iFit algorithm implemented in the MassLynx and by HMDB

[b] Fold change was calculated by dividing the mean of the peak intensity of each metabolite from the UVB-radiated group by that of the normal group

unexposed skin in this study. Prolonged exposure to UVB radiation for 12 weeks did not affect the level of *cis*-UCA, but glutamic acid, the final product formed in the histidine and UCA metabolic pathway, was significantly increased. However, metabolism from histidine to glutamic acid does little to explain these results; therefore, we need to investigate the association between *cis*-UCA and glutamic acid in depth. Nevertheless, our results suggest that the amount of *cis*-UCA increases following UV irradiation because *trans*-UCA is progressively consumed; histidine metabolism may gradually proceed over time to maintain the ratio of *trans/cis* isomers. Consistent with the increase in *cis*-UCA, with UVB irradiation, the amount of histamine increased at 6 weeks, but decreased at 12 weeks. Histamine also is associated with histidine metabolism and synthesized in a one-step decarboxylation reaction from histidine by histidine decarboxylase. The release of histamine immediately increased upon exposure to UV light, stimulated inflammation via interleukin-6 production in keratinocytes, and then returned to baseline within a short time (Shinoda et al. 1998). Furthermore, histamine and histamine receptor antagonists suppressed the immunosuppression induced by UVB and *cis*-UCA (Hart et al. 1997, 2002). These results demonstrate that *cis*-UCA and histamine acted as an initiator and inhibitor of UVB-induced immunosuppression, respectively, in the skin and that their increased levels gradually returned to background levels. The return of these levels to background seems to be correlated to the maintenance of homeostasis in the body and the fact that some *cis*-UCA is released and excreted systemically, given that *cis*-UCA has been detected in serum and urine after several weeks (Gibbs et al. 2008).

This study also found that the levels of the pyrimidine bases, cytidine and uridine, were increased following UVB irradiation, whereas the levels of the purine bases, inosine and hypoxanthine, were decreased. These metabolites are the most critical cellular chromophores that absorb in the UVB range. Kiehl and Ionescu (1992) demonstrated that purine nucleotide concentrations in the skin cells of psoriatic patients were abnormal; stimulation of the Krebs cycle with fumaric acid slowed purine nucleotide synthesis. Cyclobutane pyrimidine dimers, DNA lesions resulting from the photodimerization of adjacent pyrimidine bases, cause DNA damage at wavelengths <320 nm (Freeman et al. 1989). Abnormal changes in pyrimidine and purine metabolites upon exposure to UVB may lead to immune system dysfunction.

Table 3 Skin CERs significantly altered between NC and UC groups after exposure to UVB radiation for 6 and 12 weeks, as identified by NanoMate-LTQ analysis

6 weeks							12 weeks						
No.[a]	Ceramide type	MW	Total carbon	Fold change[b]	VIP	*p* value	No.[a]	Ceramide type	MW	Total carbon	Fold change[b]	VIP	*p* value
1	AS	553.5	34:1	1.56	1.53	0.001	1	AS	553.5	34:1	2.25	2.35	<0.001
2	NP	555.4	34:0	1.33	0.82	0.009	2	NP	555.4	34:0	1.52	1.13	0.001
	AdS	555.4	34:0					AdS	555.4	34:0			
6	NS	593.3	38:1	1.38	0.88	0.003	4	Nds	567.5	36:0	1.64	0.89	<0.001
7	NH	595.3	37:1	1.58	0.98	<0.001	6	NS	593.3	38:1	1.37	0.82	0.015
9	NdS	609.3	39:0	1.60	1.32	0.009	7	NH	595.3	37:1	1.72	1.15	0.001
10	NS	621.5	40:1	1.52	1.52	0.024	8	NS	607.6	39:1	2.46	1.74	0.039
12	NS	635.4	41:1	1.53	1.36	0.009	9	NdS	609.3	39:0	1.88	1.93	0.002
13	NdS	637.6	41:0	1.62	1.88	0.017	13	NdS	637.6	41:0	1.55	1.96	0.029
14	NP	639.7	40:0	1.59	1.31	0.014							
15	NS	649.4	42:1	1.63	1.85	0.009							
16	Nds	651.4	42:0	1.57	1.70	0.026							
17	NS	663.4	43:1	1.34	0.86	0.043							
18	Nds	665.4	43:0	1.55	1.50	0.007							
19	NP	667.4	42:0	1.51	1.18	0.007							
20	NS	677.6	44:1	1.51	0.98	0.016							
22	NdS	693.4	45:0	1.56	1.09	0.001							
	NH	693.4	44:1										
28	NdS	735.4	48:0	1.67	1.19	0.020							
	NH	735.4	47:1										

Variables were selected by VIP value (>0.7) and *p* value (<0.05) from OPLS-DA models

A α-hydroxy fatty acid, *N* non-hydroxy fatty acid, *S* sphingosine, *P* phytosphingosine, *dS* dihydrosphingosine, *H* 6-hydroxysphingosine, *MW* molecular weight, *VIP* variable important in the projection

[a] No. means the number of the identified CERs as shown in Table S3

[b] Fold change was calculated by dividing the mean of the peak intensity of each metabolite from the UVB-radiated group by that of the normal group

Taurine and its metabolic precursor, hypotaurine, were altered by chronic exposure to UVB radiation. In the skin, taurine prevents surfactant-induced dry and scaly skin by regulating proinflammatory cytokine release and stimulating the synthesis of skin barrier lipids, CERs, cholesterol, and free fatty acids (FFAs) (Anderheggen et al. 2006). Reduced skin levels of taurine correlate with an increase in the amount of amino acids, organic acids, sugars, and cholines and cause significantly higher sensitivity to UVB-induced immunosuppression in the taurine transporter-deficient mouse model (Rockel et al. 2007). With taurine, hypotaurine inhibits lipid peroxidation by scavenging the inhibitor OH (Tadolini et al. 1995) and further protects from cell damage by singlet oxygen (Pitari et al. 2000). Similarly, our results showed decreased taurine and increased histamine levels at 6 weeks and an increased level of hypotaurine at 12 weeks. In addition, *myo*-inositol, glucose, and maltose levels decreased when the skin was chronically exposed to UVB radiation. Yorek et al. (1998) found that *myo*-inositol accumulation was reduced by tumor necrosis factor-α in endothelial cells. Glucose deprivation resulted in a marked decrease in collagen via decreased collagen biosynthesis and enhanced collagen degradation in fibroblast cultures (Cechowska-Pasko et al. 2007). Thus, as with other metabolites, the alterations in taurine, hypotaurine, *myo*-inositol, and glucose in UVB-irradiated skin directly or indirectly influence the functions or structure of the skin.

Interestingly, in addition to histological changes in skin structure, we also found abnormal alterations in skin lipids induced by UVB irradiation. The lipids of the SC are important regulators of skin permeability. UVB irradiation causes morphological changes in SC lipids, such as separated and fragmentary lipid lamellae and amorphous electron-dense or electron-lucent material, an immediate increase in lipid peroxide content, and an inflammatory response, and it disrupts the permeability barrier function (Meguro et al. 1999; Jiang et al. 2006). With regard to changes in sterol levels, chronic UVB irradiation for 12 weeks decreased the levels of cholesterol and the cholesterol precursor, lathosterol. Picardo

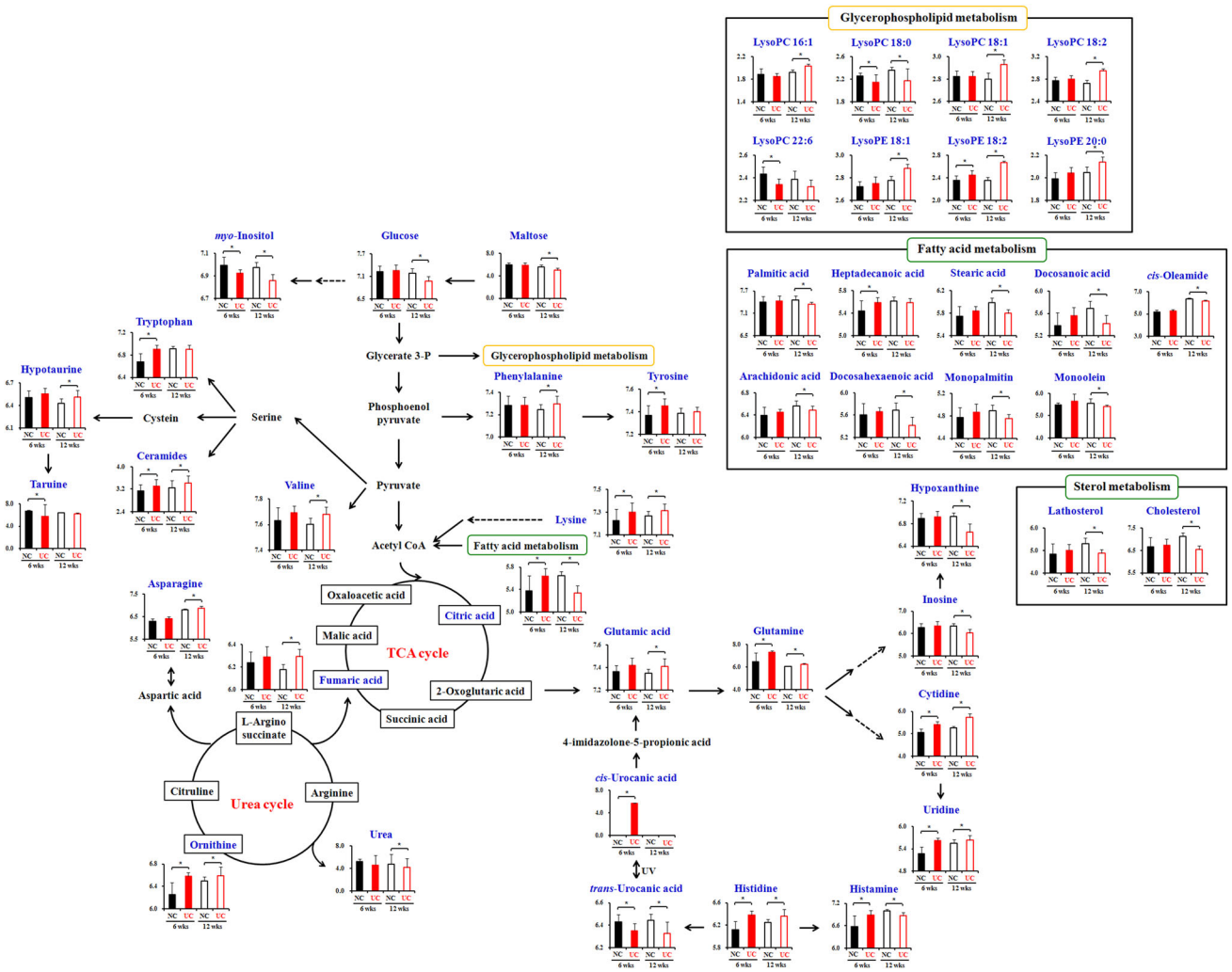

Fig. 3 The proposed metabolic pathway derived from the metabolites significantly altered in mouse skin depending on the time of exposure to UVB radiation. In the *bar* graphs, the $\log_{10}$ *peak areas* were plotted on the *y*-axis, and the experimental groups were plotted on the *x*-axis. *Filled square* 6 weeks, NC; *filled square* 6 weeks, UC; *open square* 12 weeks, NC; *open square* 12 weeks, UC. *Asterisks* indicate statistically significant differences from the UC group ($*p < 0.05$)

et al. (1991) demonstrated that cholesterol was decomposed in vivo following UV irradiation. In contrast, Knudson et al. (1939) reported that exposure of rats to sunlight and UV radiation increased the total cholesterol content of the skin. The opposing results obtained in previous studies may have derived from different experimental conditions, such as the dosage of UV radiation and the exposure time.

In addition to cholesterol, several FFAs were altered in UVB-irradiated skin at 6 and 12 weeks. Kim et al. (2010) revealed that acute and chronic UV irradiation of human skin significantly lowered the amounts of triglycerides and total FFAs by decreasing lipid metabolism and lipid synthesis. The study also showed decreased levels of saturated and unsaturated fatty acids in UVB-induced skin, suggesting that the changes in FFAs are associated with fatty acid synthesis.

A variety of CERs, a subclass of sphingolipids, are found in the SC of the skin. Among the CER classes, obtained by combining sphingoid bases and fatty acids (Pruett et al. 2008), we detected and identified 36 CERs in different six classes (NS, NdS, NP, NH, AS, and AdS) in mouse skin using NanoMate-LTQ analysis. UVB irradiation for 6 and 12 weeks increased the amount of CERs. Most intercellular lipids exist in unbound form, and it has been reported that unbound CERs play important functions in UVB-induced disruption of the skin barrier with the increase of TEWL. Takagi et al. (2004) reported increased levels of unbound CER in the SC of mice after UVB irradiation. In epidermal CERs, recent studies demonstrated that CERs with S, dS, and P sphingoid bases correlate with epidermal barrier function and TEWL (Di Nardo et al. 1998; Holland et al. 2007). These results suggest that, although an increase in CER levels

improved barrier function in UVB-exposed skin, a decrease in the amounts of other SC lipids, such as cholesterol, FFAs, and, in part, lysophospholipids, is related to skin barrier dysfunction.

Minor components of the epidermal lipid profile include glycolipids and phospholipids, especially lysoPC and lysoPE (Munder et al. 1979). We detected some lysoPCs and lysoPEs together with increased inflammatory cells in UVB-irradiated skin. The chain length and the number of double bonds in the fatty acids of lysoPCs affect their chemotactic ability (Quinn et al. 1988; Ryborg et al. 1994). A previous study by Ryborg et al. (2000) suggested that lysoPC produces skin inflammation by inducing an increase in the number of T-lymphocytes, B-lymphocytes, monocytes, and neutrophils. Additionally, Hung et al. (2012) demonstrated that administration of saturated and mono-unsaturated acyl (lysoPC 18:1) lysoPCs induced pro-inflammatory cytokines; furthermore, unsaturated acyl lysoPC 20:4 and lysoPC 22:6 significantly inhibited 1-palmitoyl (C16:0) lysoPC-induced inflammation. In addition, it has been reported that 1-linoleoyl (C18:2) lysoPC exhibits cytotoxicity through ROS formation accompanied by extracellular signal-regulated kinase activation and related inflammatory cytokine induction in macrophages (Park et al. 2009). Our study showed significantly increased levels of eight metabolites, including saturated, mono-unsaturated, and poly-unsaturated acyl lysoPCs. Compared with information on the effects of lysoPC and other phospholipids, information concerning lysoPE as a bioactive lipid is sparse, particularly in the skin. Recently, the anti-inflammatory potential of poly-unsaturated acyl lysoPE was demonstrated in a zymosan A-induced peritonitis model (Hung et al. 2011).

Considering the histological and clinical changes and the metabolites in photodamaged skin following UVB irradiation—assessed by a combination of MS analytic techniques—we propose a metabolite-based metabolic pathway between skin and UVB radiation in accordance with the exposure period (Fig. 3). *cis*-UCA and cholesterol showed the largest changes at weeks 6 and 12, respectively, indicating their potential as candidate biomarkers related to the regulation of skin photodamage. However, further biochemical and molecular studies on the relationship between UVB radiation and altered metabolites are needed to evaluate and confirm the direct effects and the metabolic pathway in depth. Nevertheless, this study suggests that a comprehensive metabolomic approach for determining the regulatory metabolites of UV-induced skin will lead to a better understanding of the relationship between skin and UV radiation and of UV-related diseases.

5 Concluding remarks

In conclusion, prolonged chronic exposure to UVB light may have a great influence on skin by altering metabolites related to skin structure, especially in the SC, suggesting that the changed metabolites are potential biomarkers for skin diseases caused by UVB irradiation. Among them, *cis*-UCA and cholesterol showed the most dramatic increase and decrease at 6 and 12 weeks, respectively.

Acknowledgments This study was supported by a grant from the Korea Healthcare Technology R&D Project (Grant No. A103017), Ministry of Health and Welfare, and by the Korea Basic Science Institute (Grant No. T33409).

References

Abaffy, T., Duncan, R., Riemer, D. D., et al. (2010). Differential volatile signatures from skin, naevi and melanoma: A novel approach to detect a pathological process. *PLoS ONE, 5*, e13813.

Anderheggen, B., Jassoy, C., Waldmann-Laue, M., Förster, T., Wadle, A., & Doering, T. (2006). Taurine improves epidermal barrier properties stressed by surfactants—A role for osmolytes in barrier homeostasis. *Journal of Cosmetic Science, 57*, 1–10.

Bellon, G., Chaqour, B., Wegrowski, Y., Monboisse, J. C., & Borel, J. P. (1995). Glutamine increases collagen gene transcription in cultured human fibroblasts. *Biochimica et Biophysica Acta, 1268*, 311–323.

Berneburg, M., Plettenberg, H., & Krutmann, J. (2000). Photoaging of human skin. *Photodermatology, Photoimmunology and Photomedicine, 16*, 239–244.

Boros, L. G., Brackett, D. J., & Harrigan, G. G. (2003). Metabolic biomarker and kinase drug target discovery in cancer using stable isotope-based dynamic metabolic profiling (SIDMAP). *Current Cancer Drug Targets, 3*, 445–453.

Cechowska-Pasko, M., Pałka, J., & Bańkowski, E. (2007). Glucose-depleted medium reduces the collagen content of human skin fibroblast cultures. *Molecular and Cellular Biochemistry, 305*, 79–85.

Chaqour, B., Bellon, G., Seite, S., Borel, J. P., & Fourtanier, A. (1997). All-*trans*-retinoic acid enhances collagen gene expression in irradiated and non-irradiated hairless mouse skin. *Journal of Photochemistry and Photobiology B: Biology, 37*, 52–59.

Dehaven, C. D., Evans, A. M., Dai, H., & Lawton, K. A. (2010). Organization of GC/MS and LC/MS metabolomics data into chemical libraries. *Journal of Cheminformatics, 2*, 9.

Di Nardo, A., Wertz, P., Giannetti, A., & Seidenari, S. (1998). Ceramide and cholesterol composition of the skin of patients with atopic dermatitis. *Acta Dermato Venereologica, 78*, 27–30.

Dioguardi, F. S. (2008). Nutrition and skin. Collagen integrity: A dominant role for amino acids. *Clinics in Dermatology, 26*, 636–640.

Freeman, S. E., Hacham, H., Gange, R. W., Maytum, D. J., Sutherland, J. C., & Sutherland, B. M. (1989). Wavelength dependence of pyrimidine dimer formation in DNA of human skin irradiated in situ with ultraviolet light. *Proceedings of the National Academy of Sciences of the United States of America, 86*, 5605–5609.

Gibbs, N. K., Tye, J., & Norval, M. (2008). Recent advances in urocanic acid photochemistry, photobiology and photoimmunology. *Photochemical & Photobiological Sciences, 7*, 655–667.

Halket, J. M., Waterman, D., Przyborowska, A. M., Patel, R. K., Fraser, P. D., & Bramley, P. M. (2005). Chemical derivatization and mass spectral libraries in metabolic profiling by GC/MS and LC/MS/MS. *Journal of Experimental Botany, 56*, 219–243.

Hart, P. H., Jaksic, A., Swift, G., Norval, M., el-Ghorr, A. A., & Finlay-Jones, J. J. (1997). Histamine involvement in UVB- and *cis*-urocanic acid-induced systemic suppression of contact hypersensitivity responses. *Immunology, 91*, 601–608.

Hart, P. H., Townley, S. L., Grimbaldeston, M. A., Khalil, Z., & Finlay-Jones, J. J. (2002). Mast cells, neuropeptides, histamine, and prostaglandins in UV-induced systemic immunosuppression. *Methods, 28*, 79–89.

Holland, W. L., Brozinick, J. T., Wang, L. P., et al. (2007). Inhibition of ceramide synthesis ameliorates glucocorticoid-, saturated-fat-, and obesity-induced insulin resistance. *Cell Metabolism, 5*, 167–179.

Hu, C., van der Heijden, R., Wang, M., van der Greef, J., Hankemeier, T., & Xu, G. (2009). Analytical strategies in lipidomics and applications in disease biomarker discovery. *Journal of Chromatography B, Analytical Technologies in the Biomedical and Life Sciences, 877*, 2836–2846.

Hung, N. D., Kim, M. R., & Sok, D. E. (2011). 2-Polyunsaturated acyl lysophosphatidylethanolamine attenuates inflammatory response in zymosan A-induced peritonitis in mice. *Lipids, 46*, 893–906.

Hung, N. D., Sok, D. E., & Kim, M. R. (2012). Prevention of 1-palmitoyl lysophosphatidylcholine-induced inflammation by polyunsaturated acyl lysophosphatidylcholine. *Inflammation Research, 61*, 473–483.

Jiang, S. J., Chen, J. Y., Lu, Z. F., Yao, J., Che, D. F., & Zhou, X. J. (2006). Biophysical and morphological changes in the stratum corneum lipids induced by UVB irradiation. *Journal of Dermatological Science, 44*, 29–36.

Kiehl, R., & Ionescu, G. (1992). A defective purine nucleotide synthesis pathway in psoriatic patients. *Acta Dermato Venereologica, 72*, 235–253.

Kim, E. J., Jin, X. J., Kim, Y. K., et al. (2010). UV decreases the synthesis of free fatty acids and triglycerides in the epidermis of human skin in vivo, contributing to development of skin photoaging. *Journal of Dermatological Science, 57*, 19–26.

Kim, H. Y., Park, H. M., & Lee, C. H. (2012). Mass spectrometry-based chemotaxonomic classification of *Penicillium* species (*P. echinulatum*, *P. expansum*, *P. solitum*, and *P. oxalicum*) and its correlation with antioxidant activity. *Journal of Microbiol Methods, 90*, 327–335.

Kligman, L. H. (1989). The ultraviolet-irradiated hairless mouse: a model for photoaging. *Journal of the American Academy of Dermatology, 21*, 623–631.

Knudson, A., Sturges, S., & Bryan, W. R. (1939). Cholesterol content of skin, blood, and tumor tissue in rats irradiated with ultraviolet light. *Journal of Biological Chemistry, 128*, 721–727.

Lappin, M. B., el-Ghorr, A., Kimber, I., & Norval, M. (1995). The role of *cis*-urocanic acid in UVB-induced immunosuppression. *Advances in Experimental Medicine and Biology, 378*, 211–213.

Lee, S., Do, S. G., Kim, S. Y., Kim, J., Jin, Y., & Lee, C. H. (2012). Mass spectrometry-based metabolite profiling and antioxidant activity of *Aloe vera* (*Aloe barbadensis* Miller) in different growth stages. *Journal of Agriculture and Food Chemistry, 60*, 11222–11228.

Legat, F. J., & Wolf, P. (2006). Photodamage to the cutaneous sensory nerves: Role in photoaging and carcinogenesis of the skin? *Photochemical & Photobiological Sciences, 5*, 170–176.

Liu, Y., Lin, Z. B., Tan, G. G., et al. (2013). Metabonomics studies on potential plasma biomarkers in rats exposed to ionizing radiation and the protective effects of *Hong Shan* capsule. *Metabolomics, 9*, 1082–1095.

Meguro, S., Arai, Y., Masukawa, K., Uie, K., & Tokimitsu, I. (1999). Stratum corneum lipid abnormalities in UVB-irradiated skin. *Photochemistry and Photobiology, 69*, 317–321.

Moloney, S. J., Edmonds, S. H., Giddens, L. D., & Learn, D. B. (1992). The hairless mouse model of photoaging: Evaluation of the relationship between dermal elastin, collagen, skin thickness and wrinkles. *Photochemistry and Photobiology, 56*, 505–511.

Munder, P. G., Modolell, M., Andreesen, R., Weltzien, H. U., & Westphal, O. (1979). Lysophosphatidylcholine (lysolecithin) and its synthetic analogues. Immunemodulating and other biologic effects. *Springer Seminars in Immunopathology, 2*, 187–203.

Narayanan, D. L., Saladi, R. N., & Fox, J. L. (2010). Ultraviolet radiation and skin cancer. *International Journal of Dermatology, 49*, 978–986.

Norval, M., Simpson, T. J., & Ross, J. A. (1989). Urocanic acid and immunosuppression. *Photochemistry and Photobiology, 50*, 267–275.

Park, C. H., Kim, M. R., Han, J. M., Jeong, T. S., & Sok, D. E. (2009). Lysophosphatidylcholine exhibits selective cytotoxicity, accompanied by ROS formation, in RAW 264.7 macrophages. *Lipids, 44*, 425–435.

Picardo, M., Zompetta, C., De Luca, C., et al. (1991). Role of skin surface lipids in UV-induced epidermal cell changes. *Archives of Dermatological Research, 283*, 191–197.

Pitari, G., Duprè, S., Spirito, A., Antonini, G., & Amicarelli, F. (2000). Hypotaurine protection on cell damage by singlet oxygen. *Advances in Experimental Medicine and Biology, 483*, 157–162.

Pruett, S. T., Bushnev, A., Hagedorn, K., et al. (2008). Biodiversity of sphingoid bases ("sphingosines") and related amino alcohols. *Journal of Lipid Research, 49*, 1621–1639.

Quinn, M. T., Parthasarathy, S., & Steinberg, D. (1988). Lysophosphatidylcholine: A chemotactic factor for human monocytes and its potential role in atherogenesis. *Proceedings of the National Academy of Sciences of the United States of America, 85*, 2805–2809.

Rockel, N., Esser, C., Grether-Beck, S., et al. (2007). The osmolyte taurine protects against ultraviolet B radiation-induced immunosuppression. *Journal of Immunology, 179*, 3604–3612.

Ryborg, A. K., Deleuran, B., Søgaard, H., & Kragballe, K. (2000). Intracutaneous injection of lysophosphatidylcholine induces skin inflammation and accumulation of leukocytes. *Acta Dermato Venereologica, 80*, 242–246.

Ryborg, A. K., Deleuran, B., Thestrup-Pedersen, K., & Kragballe, K. (1994). Lysophosphatidylcholine: A chemoattractant to human T lymphocytes. *Archives of Dermatological Research, 286*, 462–465.

Shi, H. P., Fishel, R. S., Efron, D. T., Williams, J. Z., Fishel, M. H., & Barbul, A. (2002). Effect of supplemental ornithine on wound healing. *Journal of Surgical Research, 106*, 299–302.

Shinoda, S., Kameyoshi, Y., Hide, M., Morita, E., & Yamamoto, S. (1998). Histamine enhances UVB-induced IL-6 production by human keratinocytes. *Archives of Dermatological Research, 290*, 429–434.

Son, E. D., Choi, G. H., Kim, H., Lee, B., Chang, I. S., & Hwang, J. S. (2007). Alpha-ketoglutarate stimulates procollagen production in cultured human dermal fibroblasts, and decreases UVB-induced wrinkle formation following topical application on the dorsal skin of hairless mice. *Biological &/and Pharmaceutical Bulletin, 30*, 1395–1399.

Svobodova, A., Walterova, D., & Vostalova, J. (2006). Ultraviolet light induced alteration to the skin. *Biomedical Papers of the Medical Faculty of the University Palacký, Olomouc, Czechoslovakia, 150*, 25–38.

Tadolini, B., Pintus, G., Pinna, G. G., Bennardini, F., & Franconi, F. (1995). Effects of taurine and hypotaurine on lipid peroxidation. *Biochemical and Biophysical Research Communications, 213*, 820–826.

Takagi, Y., Nakagawa, H., Kondo, H., Takema, Y., & Imokawa, G. (2004). Decreased levels of covalently bound ceramide are associated with ultraviolet B-induced perturbation of the skin

barrier. *The Journal of Investigative Dermatology, 123*, 1102–1109.

Varghese, R. S., Cheema, A., Cheema, P., et al. (2010). Analysis of LC-MS data for characterizing the metabolic changes in response to radiation. *Journal of Proteome Research, 9*, 2786–2793.

Yorek, M. A., Dunlap, J. A., Thomas, M. J., Cammarata, P. R., Zhou, C., & Lowe, W. L, Jr. (1998). Effect of TNF-alpha on SMIT mRNA levels and *myo*-inositol accumulation in cultured endothelial cells. *American Journal of Physiology, 274*, C58–C71.